Paper submitted to the IGS Symposium on *Sea Ice and Its Interactions with the Ocean, Atmosphere and Biosphere,* June 19-23, 2000, Fairbanks Alaska.

Combined satellite- and ULS-derived sea-ice flux in the Weddell Sea

MARK R. DRINKWATER[1], XIANG LIU[1], SABINE HARMS[2]

[1]*Jet Propulsion Laboratory, California Institute of Technology, 4800 Oak Grove Drive, Pasadena, CA 91109-8099, USA*
[2] *Institut fuer Meereskunde, Abt. Meeresphysik, Duesternbrooker Weg 20, 24105 Kiel, Germany*

ABSTRACT. Several years of daily microwave satellite ice-drift are combined with moored Upward Looking Sonar (ULS) ice-drafts into an ice volume flux record at points along a flux gate across the Weddell Sea, Antarctica. Monthly ice transport varies at the mooring locations from a maximum export of 0.4 $m^3 s^{-1}$ near Joinville Island to -0.4 $m^3 s^{-1}$ imported along the Fimbul and Riiser Larsen ice shelf margins. Winter peaks are observed at each end of the flux gate, where high concentrations of deformed ice are advected in and out of the basin along the coastline. The central gyre in contrast exhibits negligible seasonality and much smaller volume transports. Results indicate that gyre dynamics dominate net ice volume flux by controlling deformation and advection. During the period of overlapping ULS operation, the mean monthly integrated ice export west of the gyre center is 59 x 10^3 $m^3 s^{-1}$, and the import in the East Wind Drift is -17 x 10^3 $m^3 s^{-1}$. ULS data are compared with ERS satellite radar image pixel values to obtain an empirical relationship between ice thickness and the rate of change of backscatter with incidence angle. Resulting proxy ice-thickness data are combined with SSM/I-derived ice velocities to obtain seasonally varying estimates of net ice volume flux from 1992-98. Significant interannual variability is observed in ice volume flux expressed as freshwater transport. A maximum of 0.054 Sv is observed in 1992 with a minimum of 0.015 Sv in spring 1996. A six-year mean transport of 0.032 Sv is observed. Maximum seasonal ice export occurs in July 1992 with a minimum in November 1996. The ten-year mean area flux is 30 x 10^3 $m^2 s^{-1}$. Interannual variations in net volume flux closely follow variations in area flux with summer minima in 1990/91 and 1996/97. Maximum area transport occurs in 1991, and although this predates the ERS-1 scatterometer data, ice thickness estimates by Harms *et al.* confirm 1991 as a decadal peak in net integrated freshwater transport.

1. INTRODUCTION

Antarctic sea-ice dynamics and thermodynamics regulate surface fluxes of heat, water and momentum between atmosphere and the Southern Ocean. The general ocean circulation pattern in the Weddell Sea comprises a clockwise gyre (Deacon, 1979). Momentum and vorticity is transferred to the ice through kinematic stresses from surface wind and ultimately into the upper ocean by ice-ocean drag from ridge keels. The circulation pattern is established by long-term mean synoptic low pressure centered over the eastern Weddell Sea with additional periodic impulses from passing storm systems (Kottmeier and Sellmann, 1996). Tides and currents provide additional forces although with different frequencies and a less dominant impact on ice advection (Drinkwater, 1998a).

Ice drifts into the Weddell Sea seasonally, along the northern margin of the Fimbul ice shelf in the East Wind Drift (EWD) coastal current. The Antarctic Peninsula impedes westward drift and ice is compressed before being forced northwards out into the swift-moving eastward Antarctic Circumpolar Current (ACC). The Weddell Gyre thus provides a conveyor belt along which freshwater (in the form of ice) and small quantities of brine are transported and redistributed. Continuous ice removal from the southern Weddell Sea results in large polynyas opening along the northern margin of the Ronne-Filchner ice shelf. New-ice growth rapidly replaces ice that is advected northwards yielding enhanced freezing rates over continental shelf regions. Brine rejected during the freezing process contributes to the salination and nourishment of High Salinity Shelf Water (Carmack, 1986), driving the formation of dense, "deep" and "bottom water" as it sinks and mixes downslope from the continental shelf break (ref).

Our rudimentary knowledge of the Weddell ice drift dynamics comes from historical drifting buoy deployments since the early 80's (see Vihma *et al.*, 1996; and Kottmeier and Sellmann, 1996 for detailed reviews) and a drifting ice camp in 1992 (Gordon *et al.*, 1993). The maximum number of simultaneously reporting buoys in the Weddell Sea is however limited to 10 (in 1992). Most years are characterised by relatively sparsely distributed satellite buoy trajectories, preventing a comprehensive picture of the spatial or seasonal to interannual variability in ice drift to be established. Early Weddell Sea ice transport estimates were made by Limbert *et al.* (1989) and Vihma *et al.* (1996) on the basis of extremely sparse buoy measurements and an empirical relationship between geostrophic wind and ice drift. Each suffer from inaccuracies in the assumed spatial variability of sea-ice thickness and the assumption that ice drift conforms to the linear Thorndike and Colony (1982) model. More recently, Harms *et al.* (In Press) combined time-series ice thickness measurements from several Upward Looking Sonars (ULS) with the drift results from Kottmeier and Sellman (1996) to provide the most detailed picture of time-space variability in ice transport to-date.

New Antarctic satellite ice drift data permit more accurate ice transport and export calculations when combined with direct ice thickness measurements. In this paper, we take Harms et al (In Press) results one step further towards compiling comprehensive satellite-derived ice transport estimates in the Southern Ocean. We first combine

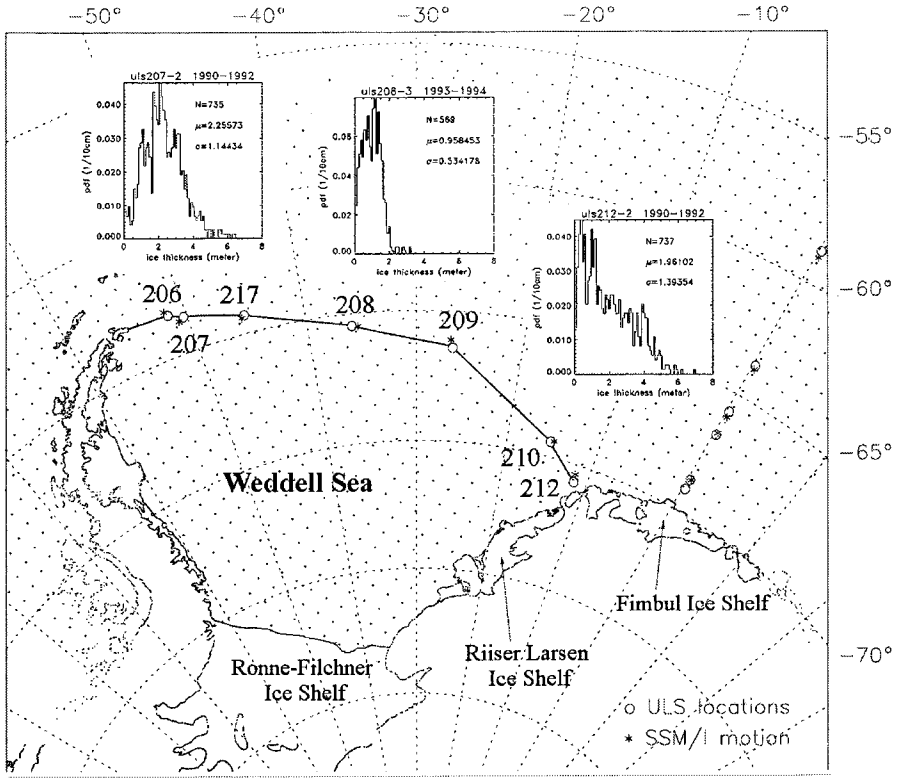

Fig. 1. Map of Weddell Sea moorings deployed by the Alfred Wegener Institut (AWI) and the flux gate *along which ice area and volume fluxes are computed. Insets show ice thickness probability distributions from 207-2, 208-3, and 212-2 during the periods indicated. Moorings along the Greenwich meridian are not discussed in this paper.*

daily satellite measurements of ice drift with daily ULS thickness records to obtain volume transport at each ULS mooring location. A new empirical relationship is developed between measured ice thickness and satellite microwave radar image data such that a proxy record of time-space variability in ice thickness can be combined with satellite-derived ice drift maps. These data are used to calculate monthly mean ice volume flux across a flux gate linking each ULS mooring location over the period 1992 - 1998.

2. DATA SETS

ULS Ice Thickness Measurements

Upward Looking Sonars (ULS) were deployed by the Alfred Wegener Institute (AWI) on twelve bottom moorings spanning the Weddell Sea using the ice breaker R.V. *Polarstern* (Strass and Fahrbach, 1998). Figure 1 indicates the locations of each of the moorings together with the conceptual "flux gate" (solid line) used in our calculations. Mooring sites were chosen to measure the time-varying inflow and outflow of ice in the Weddell Gyre. Combined data from multiple mooring deployments span the period 1990 through 1998, although there is no period when ULS operated simultaneously on all moorings. Harms *et al.* (In Press) describes in further detail all measurement periods for each of ULS moorings as well as the redeployments.

Each operable ULS instrument recorded the time-varying sea-ice draft d_i at 8 minute intervals over deployment periods ranging between 1 and 2 years. ULS draft measurement data supplied by the AWI were already binned in two different ranges (0 - 10m; and all drafts). Data binned in the cutoff range 0-10m are used by Harms *et al.* (In Press) to assess relative iceberg bias to ice thickness distribution. Both data sets were ensemble averaged over 24 hour and monthly intervals and ice draft is converted to thickness H_i using $\overline{H}_i = 0.028 + 1.012\langle d_i \rangle$ after Harms *et al.*

Ice Motion and Concentration Data

Historical Antarctic buoy array data are sparse in contrast to the Arctic basin, and therefore a Southern Ocean-wide satellite-derived ice motion data set is a primary prerequisite to understanding the response of Southern Ocean sea ice cover to meteorological and oceanographic forcing. Daily, gridded SSM/I ice motion data for this study were supplied by C. Fowler and J. Maslanik at the University of Colorado. Ice drift data is generated by tracking features in sequential pairs of Special Sensor Microwave Imager (SSM/I) 85 GHz radiometric images (~14 km resolution) using the maximum cross-correlation technique (Emery *et al.*, 1997). Resulting drift data were projected on a polar stereographic grid to facilitate overlaying vectors onto other satellite remote sensing products. SSM/I (85 GHz) ice displacements and velocities were gridded at ~90 km intervals for the period between 1987 and 1998. Antarctic ice motion results have previously been reported by Emery *et al.* (1997), Kwok *et al.* (1998) and Stammerjohn *et al.* (1998), and the comparative details of each of these ice motion products are reviewed in detail by Maslanik *et al.* (1998).

Comparisons of Weddell Sea ice drift vectors with daily buoy drift data indicate root mean square (rms) errors for x and y daily displacements of about 7.0 km. This corresponds with 1 day rms drift speed errors of ~8 cm s^{-1}. Although rms errors are clearly at the SSM/I sub-pixel scale, as Kwok *et al.* (1998) point out, daily ice motion estimates are noisy. Since comparisons with buoy data indicate Gaussian distributed errors and zero mean bias, monthly averaging

was performed to reduce ice tracking errors. Comparisons of averaged motion fields with buoy motions indicate that the standard error decreases in proportion to $1/\sqrt{n}$. The standard error for estimating monthly mean velocities is therefore 1.45 cm s^{-1} or around 18%.

SSM/I gridded measurements of ice motion are supplemented by NASA-team algorithm ice concentrations (Gloersen *et al.*, 1992) at a pixel spacing of 25 km. Contiguous regions of the ice pack with ice concentration exceeding 15% are applied as a common time-space mask for all data sets. Notably, NASA team concentrations do not correspond precisely with the period of ice coverage estimated from the ULS data. This artificially shortens the period of the year when valid ice volume flux calculations can be made. Nevertheless, this methodology removes problematic periods when adverse weather conditions or wet summer ice surfaces can cause problems to the ice tracker or may result in spurious flux estimates.

ERS Scatterometer Images

Antarctic ERS-1 and ERS-2 C-band (5.3 GHz) wind scatterometer (EScat) swath data were processed to images using the SIRF algorithm described in Drinkwater *et al.* (1993). EScat SIRF data processing yields *A* and *B* image products that describe the mean microwave backscatter of the surface over a six day imaging period. Pixel values in *A* images are normalised backscatter coefficient at 40° incidence. *B* values indicate the linear rate of decay of backscattering across the full-swath incidence-angle range of 20 to 60°. Specific characteristics of EScat images are described in further detail by Drinkwater (1998a,b); and Long and Drinkwater (1999) illustrate applications of SIRF scatterometer images to the study of polar ice.

EScat backscatter images were generated at 3-daily intervals and have an improved resolution exceeding 20 km (ref). Images are gridded with a pixel spacing of ~9km and projected onto the same polar stereographic grid as the SSM/I data. EScat images were averaged over monthly intervals for comparison with monthly mean ULS thickness estimates. In the following sections we focus on the period of overlap between SSM/I and EScat from 1992 until 1998.

3. SATELLITE ICE DRIFT

Time-varying Eulerian ice velocity $V_i(t)$ was extracted from the gridded SSM/I motion data at each of the ULS locations and combined with the corresponding ice thickness $H_i(t)$ to compute variations in ice volume transport. Monthly averaging was performed on both daily data sets prior to the multiplication.

Figure 2 indicates 1994 annual mean daily drift. The colour legend indicates drift speed and the white streamlines indicate typical trajectories of sea-ice floes in the Weddell Gyre. Converging and diverging streamlines intuitively imply ice convergence and divergence. The pattern indicates relatively rapid inflow at Kapp Norvegia focused between ULS 210 and 212, with drift speeds reaching 5 km d^{-1}. Inflowing ice decelerates in the central Gyre at its confluence with ice formed along the margin of the Ronne-Filchner ice shelves. It is compressed against the coast of the Antarctic Peninsula and forced northwards. Ice drifts parallel to the Peninsula before accelerating and turning north-eastwards as it passes Joinville Island and becomes entrained in the ACC. The highest drift speeds are observed

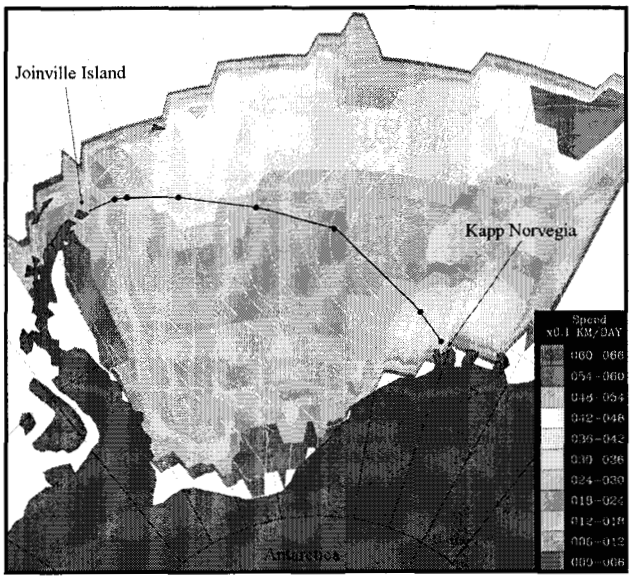

Fig. 2. Weddell Sea 1994 daily mean SSM/I-tracked ice-drift streamlines and spatial variability in drift speed.

in the marginal ice zone, where winds and currents combine to drive the ice at over 6 km d^{-1}. Zones of relatively slower ice drift are observed particularly in the coastal southern and western Weddell Sea due to transfer of internal ice stresses over distances of a few hundred kilometers from the shore.

4. ULS VOLUME TRANSPORT

Figure 1 insets show ice thickness probability distribution functions at three of seven ULS along the Weddell flux gate. Statistics are provided for the total number of daily mean values together with the overall mean and standard deviation of ice thickness during the given period of ULS operation. As reported by Strass and Fahrbach (1998), pdfs in the interior region reflect the maximum attainable thermodynamic growth thickness in a predominantly divergent ice pack. The ULS 208 pdf (Fig. 1) reports a mean thickness of 0.96 m and negligible fractions of ridged ice. In contrast, 207-2 and 212-2 report large fractions of deformed ice caused by dynamical processes such as ridging of thin ice forming in leads and polynyas. Drinkwater and Haas (1994) report *in-situ* ice thickness data along a similar flux gate during 1992 Winter Weddell Gyre Study (WWGS'92). These data indicate the same general ice characteristics across the Gyre. ULS 212-2 reports particularly deformed ice in the vicinity of Kapp Norvegia, consistent with helicopter-borne laser altimeter measurements of highly rubbled and ridged ice (Dierking, 1995) and the Polarstern becoming beset in compressed ice in that location in 1992 (Lemke, 1994). As ice circulates around the Weddell Sea thin ice grown in leads openings during wind driven or tidal ice divergence becomes rafted and ridged. The increase in mean ice thickness between ULS 212-2 and 207-2 is attributed to deformation of thin ice comprising the 0.2 m mode in inflowing ice.

Mean satellite-tracked ice drift velocities are combined with mean ULS thickness at monthly intervals in Figure 3 to compute volume transport of sea ice. The bottom panel shows the local u and v components of ice velocity $\langle Vi \rangle$, and the middle panel shows monthly scalar mean ULS thickness measurements $\langle Hi \rangle$. The upper panel indicates time-varying volume transport Φ, where $\Phi = \langle Vi \rangle \times \langle Hi \rangle$.

a.

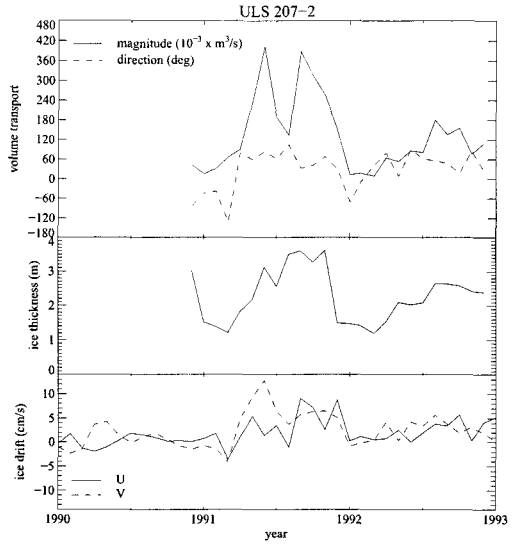

b.

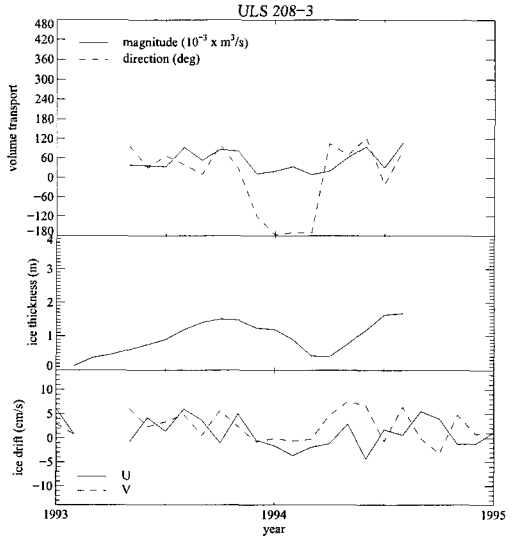

Fig. 3. Monthly ULS time series at 207 and 208 of (a) monthly mean ice volume transport, derived from combination of (b) ULS ice thickness and (c) SSM/I tracked ice velocity.

Results from ULS 207-2 and 208-3 indicate an ice volume flux toward the north-east out of the Weddell Sea throughout the winter months, with a local direction which fluctuates around a mean of ~60° (positive = clockwise). Summer reversals in flux direction occur periodically at most ULS locations with south-westerly motion noted in February 1992 at 207 (Fig. 3a), and a more extended period of south-south westerly ice recession at 208 (Fig. 3b) from January to March 1994. Strong seasonal cycles in velocity and ice thickness near to Joinville Island (206, 207, and 217) lead to correspondingly large seasonal variations in volume transport between 0 and 0.42 m^3 s^{-1}. In contrast, the central gyre exhibits a much smaller range of seasonal variability marked by a relatively gradual increase in ice thickness over the ice growth season. The smaller mean and variance in ice thickness and velocity in the interior lead to volume transports in the range 0 - 0.12 m^3 s^{-1} at mooring 208.

Figure 4 shows a comparison of seasonally varying ULS volume transport during the period of greatest overlap in ULS operation. Relative transport is computed in fixed direction of 17° and 225° for net drift out of or into the Weddell Sea, respectively. Flux magnitudes are roughly equivalent at the eastern and western extremes of the flux gate although ice is imported along a relatively narrow portion of the eastern end of the flux gate between 210 and 212 in Figure 3. Seasonal variations in the time-series of export at 207 and 217 are mirrored cycles at locations 212 and 210, suggesting that advection and ice transport in the Weddell Gyre speeds up and slows down during the winter and spring months.

A significant difference between fluxes at 212 and 210 indicates the strong decay in volume fluxes with distance from the coast noted by Strass and Fahrbach (1998) at Kapp Norvegia. Furthermore, this difference reiterates that satellite-derived ice motion data sets and models must effectively resolve strong coastal ice fluxes around the Antarctic coast for the freshwater balance to be correctly computed. Significant discrepancies are noted at the western end of the flux gate, between the results of Harms *et al.* (In Press) and our findings. The simple linear drift model they employed does not successfully account for the spatial gradient in ice velocity between ULS 207 and Joinville Island, and as a consequence they overestimate the ice volume flux at mooring 206.

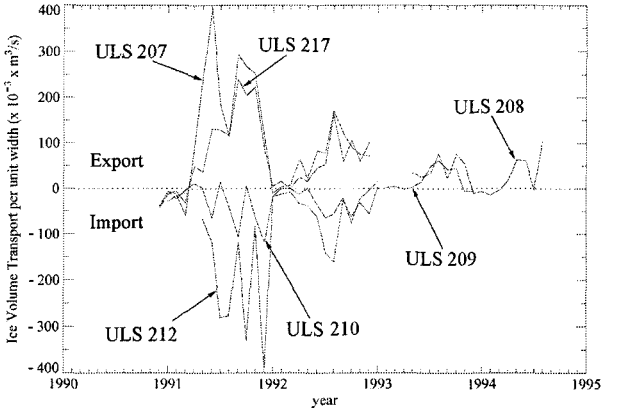

Fig. 4. Seasonal variability in ice volume transport at ULS moorings.

5. PROXY ICE THICKNESS RECORD

Without simultaneous overlapping annual cycles at each of the mooring locations it is impossible to integrate volume transport across the Weddell Sea. Harms *et al.* (In Press) find an empirical relationship between annual volume transport ice and the length of ice season, determined from independent SSM/I ice-concentrations. Although this provides a record of interannual variations in volume transport it does not tell us about the significant seasonal variations clearly apparent in the individual monthly records in Fig 3 and 4. This prompted further efforts to find an empirical relationship allowing monthly mean transports to be calculated along the entire flux gate.

Empirical Relationship

Figure 5 shows a scatter plot derived from comparisons of monthly mean *B* pixel values in EScat SIRF scatterometer images with monthly mean ice thickness at each mooring. The scatter indicates a logarithmic relationship between *B* and $\langle H_i \rangle$. The following curve was fitted to the data using least-squares regression;

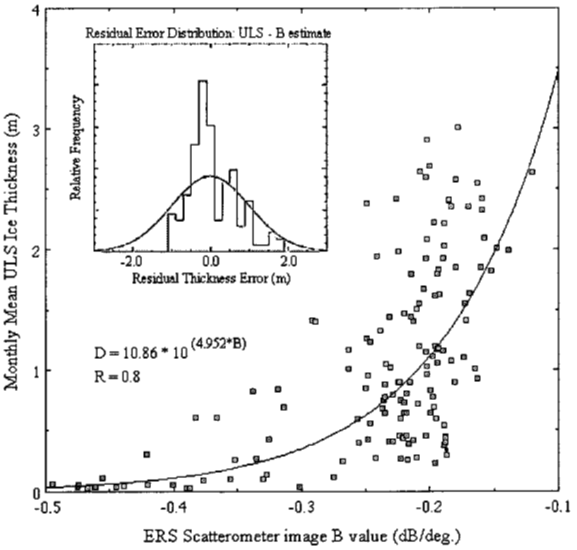

Fig. 5. Empirical relationship between Weddell Sea monthly mean ULS ice thickness and ERS Scatterometer SIRF image B pixel values. The curve indicates the exponential relationship in equation (1) fitted to the data. The inset shows the histogram of the residual errors (ULS - predicted value) and its comparison with a zero mean Gaussian error distribution.

$$\hat{D}_i = 10.86 \times 10^{4.9515B} \qquad (1)$$

where B is the monthly mean gradient in radar scattering coefficient at the ULS location. A correlation coefficient of $R = 0.8$ suggests that ~65% of the year-round variance in ice thickness can be explained by the temporal and spatial variability in C-band scatterometer image data. The rougher the ice surface becomes, the less rapidly radar backscatter decays with increasing incidence angle.

Thickness Estimate Error Analysis

Thickness estimate error is computed as the difference between monthly mean ULS ice thickness and EScat-predicted ice thickness, as $\langle H_i \rangle - \hat{D}_i$. The inset in Figure 5 shows the histogram distribution of these errors in comparison with a Gaussian distribution. The mean error is close to zero and the standard error in estimating mean ice thickness is 61 cm. This estimate error is large in comparison with the standard deviation of ice thickness σ_{Hi} (Fig. 1) or the typical standard measurement error of the monthly mean ULS thickness, defined as $\sigma_{Hi}/\sqrt{N}$. Typically, ~5000 independent ULS thickness samples are taken during a 1 month interval. For a typical mean ice thickness between 0 and 2m, this translates into a standard ULS measurement error of ± 0.03m. Though the 61cm standard error in making estimates from EScat B images is relatively large, it represents only 20% of the range of typical monthly mean thickness values (0 - 3m in Fig.1).

Figure 6 shows a comparison between estimated volume transport, calculated using equation (1) and SSM/I ice motion, and ULS volume transport Φ described in the previous section. Monthly mean data points are broken down by season to indicate whether seasonal ice conditions impact ice thickness estimation accuracy. Indeed, there is no apparent seasonal bias in transport estimates in either directional component. The standard deviation in volume transport estimates using EScat-derived proxy thickness and SSM/I ice motion is therefore 0.05 $m^3 s^{-1}$.

In general the empirical relationship has its greatest sensitivity at the thin end of the thickness distribution and the ERS scatterometer is capable of delineating areas of smooth and deformed young ice. Equation (1) slightly underestimates the thickness of perennial and deformed ice. Figure 6 shows this is likely due to winter confusion between volume- and rough-surface-scattering ice floe surfaces and the fact that undeformed perennial ice with a deep snow cover can produce a scattering signature similar to that of extremely deformed first-year ice. Summer melting in contrast provides less problems for thickness estimation from B images as it exaggerates the scattering contrast between ridged/rubbled and level ice surfaces.

Data in Figure 5 were not partitioned by season and some improvement may be possible if regionally and seasonally dependent empirical fits are obtained.

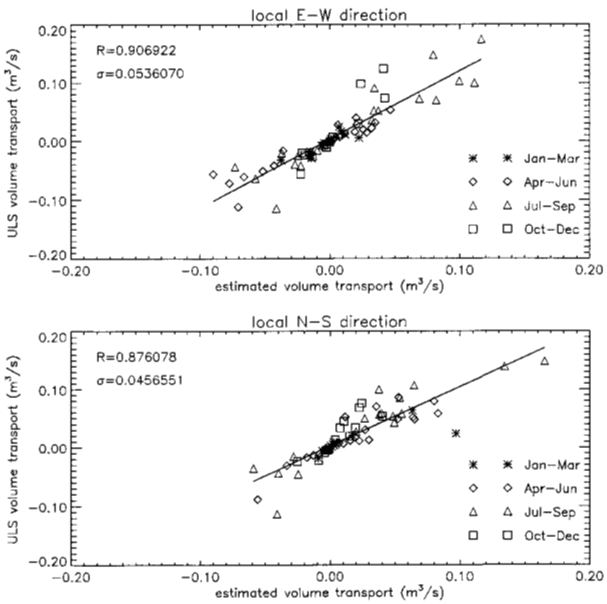

Fig. 6. Comparison of monthly mean estimates of volume transport at each ULS mooring for all ice-covered months with SSM/I ice drift, ULS ice thickness data, and EScat estimates of ice thickness.

7. INTEGRATED VOLUME FLUX

Initially we computed annual net ice volume flux orthogonal to the flux gate by (i) finite-differencing ULS measured monthly mean Φ values in Figure 4 (between moorings); (ii) performing a time integral on the resulting monthly flux to obtain annual integrated ice flux values; and (iii) summing integrated fluxes across all line segments along the flux gate. Results are also compared with those obtained by linearly interpolating to 1 metre intervals along the flux gate (as performed by Harms *et al.*), but the results did not differ significantly nor warrant the additional computational burden of interpolation.

Our finite difference results were compared with those of Harms *et al.* (In Press) in order to assess the improvement when satellite-tracked drift is incorporated in calculations of net volume flux. Their estimates rely upon a combination of the linear ice-drift model of Thorndike and Colony (driven by ECMWF winds) with the same ULS thickness data.

Consequently their results significantly overestimate net ice export and import into the Weddell Sea at moorings 206 and 212, due to strong seasonal and spatial variability in internal ice strength not captured by the simple advective model. Overall, we obtain a 20% smaller integrated volume transport of 46 x 10^3 m^3 s^{-1} for the western outflow and a 50% smaller influx of 18 x 10^3 m^3 s^{-1} across the narrow eastern coastal inflow. Our net ice flux budget orthogonal to the flux gate is therefore 46 x 10^3 m^3 s^{-1}. Since net ice flux from the Weddell Sea was computed by subtracting inflow from the outflow it appears that the overestimated Harms *et al.* net transport values partially cancel out one-another. The result is that their overall net integrated volume transport is only around 10% greater than our value.

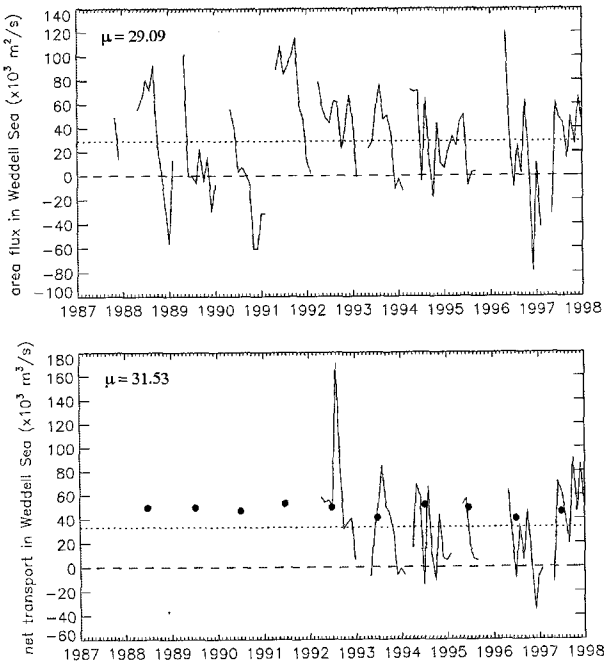

Fig. 7. Weddell Sea monthly mean values of (a) net area flux; and (b) net volume flux. Solid circles in (b) indicate annual means from Harms et al. (In Press).

Comparisons were also made with the results of using the 10m ice thickness cutoff statistics described in Section 2. A significant decrease is noted in the east-west component in volume flux at ULS 206 when the 10m cut off is used for its 1996-97 operating period. This suggests that the iceberg flux from the disintegrating Larsen ice shelf (Rott *et al.*, 1998) may have significantly biased ice thickness statistics at this mooring location. In general, however, use of a 10m ice thickness cut off only reduces volume flux by a few percent, due to icebergs having limited impact over most of the flux gate.

8. ANNUAL ICE VOLUME FLUXES

Since the AWI ULS did not operate simultaneously along the Weddell flux gate, proxy EScat ice thickness data (from Section 5) are required to calculate seasonal and interannual variability in Weddell Sea net ice-volume flux. Monthly mean results in Figure 7 indicate the seasonal and interannual variability in net area and volume flux for periods when the flux gate is covered by ice exceeding 15% concentration. Figure 7a shows a nine-year mean ice-area flux of 29 x 10^3 m^2 s^{-1} from SSM/I ice-drift data (shown as dotted line). Monthly mean thickness estimates from equation (1) are combined with the area flux to obtain the six year mean volume flux of 32 x 10^3 m^3 s^{-1} (limited to the 1992 - 1998 operation of ERS-1 and -2). This translates to an effective net mean freshwater export of 32 x 10^3 m^3 s^{-1} or 0.032 Sv (1 Sv. = 1 x 10^6 m^3 s^{-1}). To assess errors in computing net fluxes we considered the standard estimation errors for ice drift and thickness in Section 2, together with the 1σ error bound of 0.07 m^3 s^{-1} in transport in Fig. 6. We obtain errors in integrated net volume flux of about 25% of the mean monthly flux, and of the order of 5 x 10^3 m^3 s^{-1} for the annual means shown in Table 1.

Seasonal to Interannual Variability

Upper and lower panels in Figure 7 indicate the relative contributions of advection and thickness to net monthly variations in ice volume transport. Net transport typically increases rapidly from a summer minimum (when the least ice covers the basin) up to July peak values of 150 x 10^{-3} m^3 s^{-1} as a consequence of large quantities of perennial ice floes advected out of the south-western Weddell Sea (Drinkwater, 1998a). July to October values drop considerably in the Western Weddell Sea as ice convergence retards ice drift and area flux. The most rapid ice drift velocities are not normally observed in mid-winter due to increased internal ice stress when the basin is completely filled by ice. Springtime area flux falls to seasonal minimum in all years except 1997.

Table 1 shows the summary of annual mean values (based on monthly mean values in Fig. 7). It indicates that there is a significant interannual variability in both area and volume flux. The maximum area flux of 67.9 x 10^3 m^2 s^{-1} occurs in 1991. Though these measurements predate our EScat data, ice thickness estimates from Harms *et al.* also confirm a 1991 decadal peak in net ice transport. The 1990 results in contrast indicate anomalously large net southward transport during the latter part of the year, reproduced only in the spring of 1988 and 1997.

Comparative estimates of net ice export by Vihma *et al.* (1996) show considerable differences with results in Table

Table 1. Weddell Sea annual mean fluxes of ice area and volume from combined ice thickness estimates and ice drift data.

Year	1987	1988	1989	1990	1991	1992	1993	1994	1995	1996	1996
Net Area Flux (x 10^3 m^2 s^{-1})	31.2	34.6	10.3	-5.7	67.9	48.4	30.2	28.7	21.9	19.1	27.8
Net Volume Flux (x 10^3 m^3 s^{-1})	-	-	-	-	-	54.2	27.4	22.1	22.1	14.9	43.7

1. The primary drawback noted in their work, however, is their lack of information on spatial and interannual variability in ice thickness. Their estimates are as a result biased low with net ice export values for 1992, 1993 and 1994 of 22, 85, and 18 x 10^3 m^3 s^{-1} respectively.

Further comparisons are made with the annual means from Harms *et al.* (In Press) shown as solid circles in Fig. 7. Notably, their results slightly overestimate the long-term mean, which is not surprising given the tendency of the linear drift model to overestimate the advective component of the flux. More surprising perhaps is the fact that we capture significantly greater interannual variability in the net volume flux. This can only presently be explained by the extremely large seasonal variance demonstrated in this study, and the fact that their result does not capture the strong variations in the area flux.

9. CONCLUSIONS

Results in this paper are derived by applying a similar ice volume transport integration strategy to Harms *et al.* (In Press). Our data indicate that strong spatial gradients in the area flux have a significant impact upon net ice volume flux, as do strong seasonal to interannual fluctuations in ice advection and thickness. Results demonstrate that it is extremely vital to consider both spatial and temporal variability in ice drift in order to capture the true seasonal variance in sea-ice transport or freshwater flux. It is particularly timely to exploit new gridded satellite-derived ice drift data sets for this purpose.

As previous results have demonstrated, ice export is greatest at the north-western end of the flux gate near the tip of the Antarctic Peninsula and declines eastwards towards the central gyre. Ice import takes place in the coastal current entering at the east of the Weddell Sea across a narrow portion of the flux gate. Individual ULS moorings near Kapp Norvegia can indicate transports of comparable magnitude to those ULS near the tip of the Antarctic Peninsula. Periods of significant volume import appear closely related to the amount of ice convergence occurring within the coastal regime in the eastern Weddell Sea. Net sea-ice flux out of the Weddell Sea is as a consequence regulated by the quantity of thick ice carried into the basin.

Direct flux estimates presented in Section 7 should be considered with care. It was necessary to assume negligible interannual flux variability in order to combine non-overlapping ULS data from all moorings. We now know this not to be an appropriate assumption. An identical methodology to that of Harms *et al.* was applied simply to make possible direct comparisons between net fluxes with and without satellite ice-drift data. ULS thickness data used in this integration were obtained from mixed periods between 1991 and 1997. Data from ULS 207, 217 and 212 from the period 1991-1992 (Fig. 4), in particular, indicate years and seasons with anomalously large transports. The resulting integrated net flux of 46 x 10^3 m^3 s^{-1} is therefore biased high relative to the estimated six year mean of 32 x 10^3 m^3 s^{-1}.

Interannual variations in area and volume flux appear to indicate multiyear cycles characterized by positive and negative anomalies with wavelengths of several years. This is not surprising given other supporting evidence for anomalies in sea-level pressure and large-scale atmospheric circulation patterns (Drinkwater, 1996). The time scales associated with resulting patterns of freshwater depletion and salt enrichment make it imperative that continued systematic, long-term *in-situ* observations are made of ocean and ice properties in this region. This requires carefully designed deployments of moored sensors such as the AWI ULS data exploited in this study. The demonstrated relationship between ice thickness and satellite data is undoubtedly limited by the highly variable regional and seasonal characteristics of Weddell Sea ice. Future calculations of net ice volume flux will require continued seasonal to interannual measurements from such moored ULS sensors such that an accurate satellite-derived proxy records for ice thickness can be suitably be developed. Only then can detailed satellite-derived ice drift data and thickness estimates be fully exploited for Southern Ocean wide freshwater and salt balance calculations.

In future extensions of this work, we plan to compute fluxes using SSM/I grid point measurements of ice velocity at 100 km intervals along the flux gate, rather than finite differencing between ULS mooring locations. This additional information on the spatial variability in ice drift and thickness will undoubtedly change the preliminary results shown here. Such data will allow much more accurate Weddell Sea budget estimates for salt and freshwater than could previously be made with sparsely deployed buoy arrays.

ACKNOWLEDGMENTS

Eberhard Fahrbach and Volker Strass and the Alfred Wegener Institute are sincerely thanked for allowing access to these ULS data. M.D. and X.L. conducted this research at the Jet Propulsion Laboratory, California Institute of Technology under contract to the National Aeronautics and Space Administration. Funding support was provided by NASA Code YS through RTOP Grant 622-82-31. ERS wind scatterometer data were provided by IFREMER and analyzed as part of ESA Project AO2.USA.119.

REFERENCES

Carmack, E.C., 1986. Circulation and Mixing in Ice-Covered Waters, In Untersteiner, N. (Ed.), *The Geophysics of Sea Ice*, 641-712, Plenum Press.

Deacon, G., The Weddell Gyre, *Deep Sea Res.*, 26, 981-998, 1979.

Dierking, W., 1995. Laser profiling of the ice surface topography during the Winter Weddell Gyre Study 1992, *J. Geophys. Res.*, 100, C3, 4807-4820.

Drinkwater, M.R., 1998a Satellite Microwave Radar Observations of Antarctic Sea Ice. In C. Tsatsoulis and R. Kwok (Eds.), *Analysis of SAR Data of the Polar Oceans*, Chapt. 8, 147-187, Springer-Verlag, Berlin.

Drinkwater, M.R., 1998b. Active Microwave Remote Sensing Observations of Weddell Sea Ice. In M.O. Jeffries (Ed.) Antarctic Sea Ice: Physical Processes, Interactions and Variability, *Antarctic Research Series.*, 74, 187-212, American Geophysical Union, Washington, D.C.

Drinkwater, M.R., 1996. Satellite Microwave Radar Observations of Climate-Related Sea-Ice Anomalies, *Bull. Am. Met. Soc., Proc. Workshop on Polar Processes in Global Climate*, 13-15 Nov., 1996, 115-118.

Drinkwater, M.R., and Haas, C., 1994. Snow, Sea-ice and Radar Observations during ANT X/4: Summary Data Report, *AWI Berichte aus dem Fachbereich Physik*, 53 Alfred Wegener Institut für Polar- and Meeresforschung, 58pp.

Drinkwater, M.R., D.G. Long, and D.S. Early, 1993. Enhanced Resolution Scatterometer Imaging of Southern Ocean Sea Ice, *ESA Journal*, 17, 307-322.

Emery, W.J., C.W. Fowler and J.A. Maslanik, 1997. Satellite-Derived Maps of Arctic and Antarctic Sea Ice Motion: 1988-1994, *Geophys. Res. Lett.*, 24, 8, 897-900.

Gordon, A.L., and Ice Station Weddell Group of Principal Investigators and Chief Scientists, Weddell Sea Exploration from Ice Station, *Eos*, 74, 121, 1993.

Gloersen, P., W.J. Campbell, D.J. Cavalieri, J.C. Comiso, C.L. Parkinson, and H.J. Zwally, 1992. Arctic and Antarctic sea ice, 1978-1987: Satellite passive-microwave observations and analysis. *NASA SP-511*, Washington DC, National Aeronautics and Space Administration.

Harms, S., E. Fahrbach, and V.H. Strass, 2000. Ice Transports in the Weddell Sea, *J. Geophys. Res.*, In Press.

Kottmeier, C., and L. Sellmann, 1996. Atmospheric and Oceanic Forcing of Weddell Sea Ice Motion, J. Geophys. Res., 101, C9, 20809-20824.

Kwok, R., A. Schweiger, D.A. Rothrock, S. Pang, and C. Kottmeier, Sea Ice Motion from Satellite Passive Microwave Imagery Assessed with ERS SAR and Buoy Motions. *J. Geophys. Res.*, 103, C4, 8191-8214, 1998.

Lemke, P. *ed..*, 1994. The Expedition Antarktis X/4 of R/V "Polarstern" in 1992, *Reports on Polar Research*, 140, Alfred-Wegener-Institut für Polar- und Meeresforschung, D-27568, Germany, 90pp.

Limbert, D.W.S., S.J. Morrison, C.B. Sear, P. Wadhams, and M.A. Rowe, 1989. Pack-ice Motion in the Weddell Sea in Relation to Weather Systems and Determination of a Weddell Sea Ice Budget, *Ann. Glaciol.*, 12, 104-112.

Long, D.G., and M.R. Drinkwater, 1999. Cryosphere Applications of NSCAT Data, *IEEE Trans. Geosci. and Remote Sens.*, Vol. 37, No. 3, 1671-1684.

Maslanik, J., T. Agnew, M.R. Drinkwater, W. Emery, C. Fowler, R. Kwok, and A. Liu, 1998. Summary of Ice-Motion Mapping Using Passive Microwave Data. Report prepared for the Polar Data Advisory Group, *NASA Snow and Ice Distributed Active Archive Center, National Snow and Ice Data Center*, Special Pub. 8, Boulder, Colorado, 25 pp.

Rott, H., W. Rack, T. Nagler, and P. Skvarka, 1998. Climatically induced retreat and collapse of the northern Larsen Ice Shelf, Antarctic Peninsula, Annals of Glac. 27, 86-92.

Stammerjohn, S., R. Smith, M.R. Drinkwater, and X. Liu, 1998. Variability in Sea-Ice Coverage and Ice-motion Dynamics in the PAL LTER Study Region West of the Antarctic Peninsula, *Proc. IGARSS '98*, Seattle, Washington, 6-10 July, 1998., IEEE Catalog # 98CH36174, Vol. 3, 1434-1436.

Strass, V.H, and E. Fahrbach, 1998. Temporal and Regional Variations of Sea Ice Draft and Coverage in the Weddell Sea Obtained from Upward Looking Sonars, In M.O. Jeffries (Ed.) Antarctic Sea Ice: Physical Processes, Interactions and Variability, *Antarctic Research Series.*, 74, 123-139, American Geophysical Union, Washington, D.C..

Thorndike, A.S., and R. Colony, 1982. Sea Ice Motion in Response to Geostrophic Winds, *J. Geophys. Res.*, 87, 5845-5852.

Vihma, T., J. Launiainen, and J. Uotila, 1996. Weddell Sea Ice Drift: Kinematics and Wind Forcing, *J. Geophys. Res.*, 100, C9, 18503-18515.